SCIENCE CHINA
Physics, Mechanics & Astronomy

•Article•

May 2019 Vol. 62 No. 5: 954611
https://doi.org/10.1007/s11433-018-9332-2

Existence criteria and validity of plate models for graphene-like materials

JiaPeng Chen[1], and Biao Wang[2,3*]

[1] *School of Electronics and Information Technology, Sun Yat-Sen University, Guangzhou 510275, China;*
[2] *School of Physics, Sun Yat-Sen University, Guangzhou 510275, China;*
[3] *Sino-French Institute of Nuclear Engineering and Technology, Sun Yat-Sen University, Guangzhou 510275, China*

Received October 21, 2018; accepted November 23, 2018; published online March 20, 2019

Graphene-like (GL) materials have enriched the application prospects of two-dimensional materials by virtue of their various structures and properties. However, the following theoretical issues remain unsolved: how can stable GL materials exist and is plate idealization valid for any GL materials? Here we answer these questions based on an atomistic potential-based approach. The existence criteria for GL materials with three common structures, including planar honeycomb (PH), buckled honeycomb (BH), and honeycomb MX_2 (2H-MX_2) structures, were established. Moreover, the validity of classic linear-elastic plate models for these materials was examined. A validity factor, which represents the validity of using thin plate models to investigate the overall mechanical response of GL sheets, was defined. We determined that 2H-MX_2 sheets can approximately be modeled as thin plates for arbitrary loadings, unlike PH and BH sheets.

grapheme-like material, existence criterion, plate idealization

PACS number(s): 62.25.+g, 45.05.+x, 46.70.De

Citation: J. P. Chen, and B. Wang, Existence criteria and validity of plate models for graphene-like materials, Sci. China-Phys. Mech. Astron. **62**, 954611 (2019), https://doi.org/10.1007/s11433-018-9332-2

1 Introduction

Two-dimensional (2-D) materials have attracted tremendous attention from academia and industry since the discovery of graphene [1]. Graphene is a single-atom-thick sheet with carbon atoms arranged in a planar honeycomb (PH) lattice with sp^2 hybridization. Such unique structure guarantees ultrahigh carrier mobility, flexibility, and thermal conductivity; hence, graphene is considered a potential candidate for next-generation electronic applications [2]. However, the ideal graphene sheet is unsuitable for being directly applied to logic devices because of the half-metallicity [3]. Complex band-gap engineering is thus required to tune the electronic properties of graphene without significantly changing the other properties. To broaden the families and application ranges of 2-D materials, scientists started to explore graphene-like (GL) materials [4] that have structures analogous to graphene. To date, several kinds of GL materials have been successfully synthesized or exfoliated [5-13], such as silicene [5], 2-D h-BN [6], and single-layer transition metal dichalcogenides (SLTMDs) [7]. These materials present a various electronic properties ranging from metallic to insulating. For instance, a free-standing silicene exhibits the characteristic of a conductor, while 2-D h-BN is an insulator and most SLTMDs are semiconductors [14]. The diversity of conductivity results in a broad range of applications of GL materials in electronics, including insulating layers, transistors, flexible display screens and solar

*Corresponding author (email: wangbiao@mail.sysu.edu.cn)

cells [15-17].

Researchers have devoted considerable efforts to explore the structural stability of GL materials through theoretical and experimental analyses [18-20]. These works have verified that the GL materials have various structures that can be classified into several categories [14]. Planar honeycomb (PH), buckled honeycomb (BH), and honeycomb MX_2 (2H-MX_2) structures are the three most common structures under current investigation. These structures are illustrated in Figure 1. Although the morphology of GL materials has been extensively studied, the determinant of their stable existence remains unclear. The structures of materials in the ground state totally rely on their ways of bonding (e.g., a stable PH configuration is ascribed to sp^2 hybridization, and a material with BH structure exhibits the sp^2-sp^3 hybridization). Nonetheless, the relation between the bonding nature and existence of GL materials has not been studied. At present, a few unsolved issues remain on this topic: Can interatomic bonding-related requirements for existence of GL materials be found? What are the exact formulae of these requirements? How the bonding nature stabilizes GL materials?

The rise of micro- and nano-mechanics, involving the development of multi-scale modeling, experimental techniques, and interdisciplinary studies, has expanded the content of mechanics [21,22]. Researchers strongly desire to take advantage of the well-developed continuum mechanics approach to investigate the mechanical behavior of nanoscale materials [23-28]. Actually, some of continuum mechanics relationships may no longer be retained at the nanoscale level. For instance, different configuration descriptions of the surface or the bulk thermo-hyperelastic constitutive equations of nanostructured materials are not the same even in cases of infinitesimal deformation due to the existence of surface residual stresses [29]. Visually, 2-D materials can be modeled as thin plates. To this end, a thickness that links 2-D discrete systems to continuum plate models, has to be defined. Two kinds of thickness with two different definitions are reported [30]. First, thickness is directly defined by interlayered spacing d of corresponding layered structure (e.g., d = 0.34 nm for h-BN and d = 0.62 nm for MoS_2). However, such definition of thickness only applies to systems with in-plane deformation. The second is effective thickness, whose definition considers bending deformation. The mathematical formulation is related to the ratio of bending to in-plane stiffness by referring to the relation between the elastic constant and bending stiffness matrices of thin plates. The two definitions generally give the scattered values of thickness and lead to Yakobson's paradox [31]. Such divergence is reduced as the number of atomic layer increases [32,33]. However, for arbitrary loadings, using thin plate models to predict the properties of 2-D materials is usually controversial. Indeed, the effective thickness of graphene depends on types of loading [30]; as such, a universal constant thickness cannot be defined. In other words, for arbitrary loadings, thin plate idealization of graphene is of failure. The following questions arise: Can GL materials be strictly idealized as thin plates? If the answer is no, then what kinds of GL materials can be approximately regarded as thin plates when the system subject to arbitrary loadings?

Recently, we have analytically established an existence criterion for low-dimensional materials directly from the interatomic potential by considering their exotic geometrical features [34]. The present study aims to answer existing issues by using this approach. The paper is organized as follows. In sect. 2, we briefly describe the method and introduce the formalism of interatomic potentials and the derivation process of deformation-structural parameter relations to gain analytical results. The existence criteria for GL materials

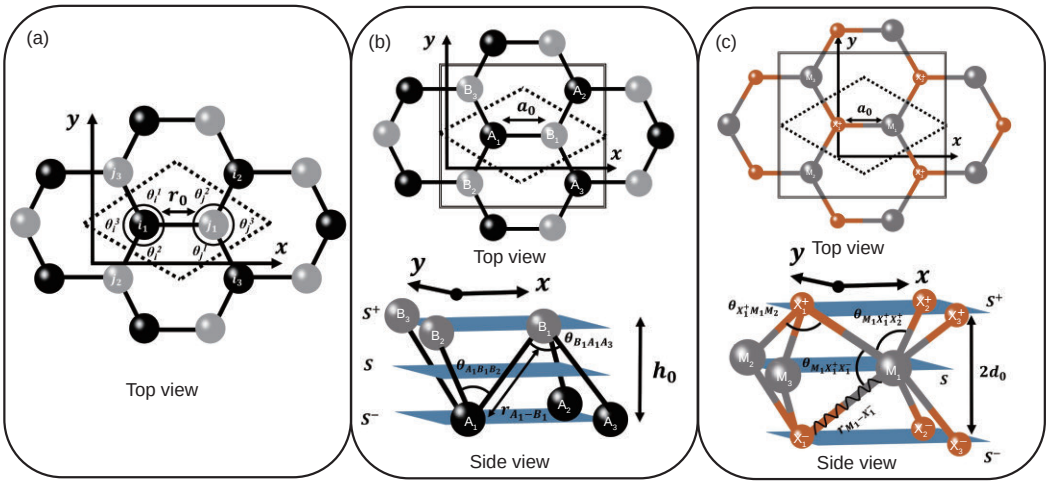

Figure 1 (Color online) Three configurations of graphene-like 2-D materials. The unit cells are separately highlighted by dotted rhombuses. (a) The top view of PH structure. The top views and side views of atoms in the square of (b) BH and (c) 2H-MX_2 structures, respectively. In the BH structure, the neighboring atoms are located in different parallel planes with the distance between these two planes being h_0 (height of buckling). The 2H-MX_2 structure has three atomic planes, in which one plane of M atoms is sandwiched by the two other planes of X atoms.

with the three structures shown in Figure 1 are derived in sect. 3 to establish the requirements of the existence of such materials. The requirements for 2H-MX_2 are easier to be satisfied than those for PH and BH materials. In sect. 4, we discuss the validity of classical linear-elastic thin plate models by utilizing the results in sect. 3. The global behavior of 2H-MX_2 sheets, especially of single-layer NbS_2, is similar to that of classical thin plates for arbitrary loadings. The breakdown of thin plate models occurs in PH and BH sheets, consistent with the results of theoretical studies to some extents [32,33].

2 Methodology

2.1 Introduction of the existence criterion for 2-D materials

Assuming that a crystal lies in a huge isochoric medium without any external field (e.g., pressure, electromagnetic field) applied, the Helmholtz free energy F of the crystal should be kept to a minimum for its structure to be in the state of thermodynamic equilibrium under isothermal condition [35,36]. F can be expressed as:

$$F = \Phi - kT\ln Z_v, \tag{1}$$

where Φ is the total interatomic potential of the crystal, k is the Boltzmann constant, T is the thermodynamic temperature, and Z_v is the part of the partition function depending on vibration. Applying eq. (1) directly is not easy, because the complete phonon spectrum is difficult to derive analytically. The temperature effect should be eliminated to provide requirements that clarify the existence of 2-D materials. In low-temperature limit, the free energy F becomes approximately identical with the total interatomic potential Φ. Thus, the existence criterion for 2-D materials with a specific structure is established by the following two steps [34].

First, the extreme value conditions of the Φ of 2-D materials are derived. These conditions provide a set of equations on the specific structures of materials in the equilibrium state, and the geometric parameters of the structures (e.g., bond length r_b, bond angle θ) can be derived by solving these equations.

Second, the conditions of the mechanical stability of 2-D materials are derived. Born [35] proposed that a crystalline solid must be mechanically stable. Otherwise, the solid would exhibit a structural phase transition, or even transform into a liquid or gas. For 3-D materials, strain tensor $\{\varepsilon\}$ characterizes the macroscopic perturbation. The conditions of mechanical stability of materials can be derived from the positive definiteness of the quadratic terms of ϕ with respect to $\{\varepsilon\}$. Unlike 3-D materials, 2-D materials are subject to in-plane strain $\{\varepsilon\}=\{\varepsilon_{xx}, \varepsilon_{yy}, \varepsilon_{xy}\}$ and curvature $\{\kappa\} = \{\kappa_{xx}, \kappa_{yy}, \kappa_{xy}\}$, which are caused by stretching and bending, respectively. The mechanical stability conditions of 2-D materials can be derived from the positive definiteness of the quadratic terms of Φ with respect to $\{\varepsilon\}$ and $\{\kappa\}$. These terms are defined as $\Phi_{e_{\alpha\beta},e_{\gamma\delta}} = \left(\partial^2\phi / \partial e_{\alpha\beta}\partial e_{\gamma\delta}\right)_0$, where $e_{\alpha\beta}$ and $e_{\gamma\delta}$ denote the elements of $\{\varepsilon\}$ or $\{\kappa\}$. The conditions are consequently expressed in the form of inequalities for several parameters of Φ. For GL materials, changes in the total potential Φ are equivalent when the systems are separately subjected to two equal and opposite curvatures. Therefore, in the series expansion of Φ, the odd power of κ vanishes. As such, for infinitesimal deformation, strain and curvature are decoupled in energy. The quadratic terms of Φ with respect to $\{\varepsilon\}$ and $\{\kappa\}$ form a 6×6 block diagonal matrix:

$$\mathbf{M} = N\begin{bmatrix}\mathbf{C} & \mathbf{0}\\ \mathbf{0} & \mathbf{D}\end{bmatrix}, \tag{2}$$

where N denotes the number of unit cells. **C** and **D** are 3×3 matrices and their elements are $\Phi_{\{\varepsilon\},\{\varepsilon\}}/N$ and $\Phi_{\{\kappa\},\{\kappa\}}/N$, respectively. As a result, the positive definiteness of **C** and **D** represents the need for mechanical stability of GL materials. The elements of **C** and **D** consist of two kinds of parameters: derivatives of the interatomic potential with respect to the structural parameters (e.g., $\partial^2\Phi/\partial r_b{}^2$, $\partial\Phi/\partial\cos\theta$), and derivatives of the structural parameters with respect to the macroscopic deformations (e.g., $\partial^2 r_b/\partial^2 e_{\alpha\beta}$, $\partial\cos\theta/\partial e_{\alpha\beta}$). The former depends on the elements that form GL materials, and the latter can be derived analytically by constructing deformation-structural parameter relations for the materials.

The criterion constructed by the above two-step atomistic potential-based deduction can provide requirements for any 2-D material to exist. Since different kinds of atom-atom bonding possess different interatomic potential, one can clarify what kinds of atoms will form stable 2-D materials according to this criterion. Furthermore, the criterion can provide a guideline for scientists to choose a suitable interatomic potential for computer simulation of 2-D materials.

2.2 Interatomic potential

In the following derivations, a well-defined interatomic potential would be employed. The different kinds of interatomic potentials for GL materials are embedded-atom method potential [37], Stillinger-Weber (SW) potential [38] and bond-order (BO) potential [39]. Generally, the choice of these potentials in the field of atomistic modeling investigations is rather arbitrary. Here we will briefly summarize the formalisms of SW and BO potential, respectively.

2.2.1 SW potential

Among the interatomic potentials that contain multi-body (more than two) interaction, the functional form of SW po-

tential is the simplest because it has the least parameters to be fitted. The SW potential for n particles has the form [38]:

$$\Phi(1\ldots n)=\sum_i V_1(i)+\sum_{\substack{i,j\\ i<j}} V_2(i,j)+\sum_{\substack{i,j,k\\ i<j<k}} V_3(i,j,k), \tag{3}$$

where V_1 is the single-particle potential and can be considered as a constant in the absence of spatial-variation field effects. V_2 and V_3 describe the two-body and three-body interactions, respectively, and have the forms [40]:

$$\begin{aligned} V_2(i,j)&=\begin{cases} A\left(\frac{B_{ij}}{r_{ij}^4}-1\right)\mathrm{e}^{\frac{\gamma_{ij}}{r_{ij}-a}}, & r_{ij}<a,\\ 0, & r_{ij}\geq a,\end{cases}\\ V_3(i,j,k)&=\begin{cases} \epsilon\mathrm{e}^{\frac{\gamma_{ij}}{r_{ij}-a}+\frac{\gamma_{ik}}{r_{ik}-a}}\left(\cos\theta_{ijk}-\cos\theta_0\right)^2, & r_{ij},r_{ik}<a,\\ 0, & r_{ij},r_{ik}\geq a,\end{cases}\end{aligned} \tag{4}$$

where r_{ij} is the distance between atoms i and j, and θ_{ijk} is the angle between chemical bonds i-j and i-k. The parameter a represents the cut-off distance, which is generally lower than the distance of the second-nearest neighbor atoms. As a result, r_{ij} and θ_{ijk} in eq. (4) denote the bond length and bond angle of the system, respectively. A and ϵ are energy parameters, which indicate the strength of two-body and three-body interaction, respectively. θ_0 is the equilibrium value of θ_{ijk}. B and γ are length parameters, and depend on the types of the interacting particles.

According to eqs. (3) and (4), for the system without boundary effect, the potential per unit cell by assuming SW potential is

$$\begin{aligned} \frac{\Phi}{N}&=\sum_i \phi_i\left(\{r_\mathrm{b}\},\{\cos\theta_i\}\right),\\ \phi_i&=\frac{1}{2}\sum_j^{\text{Neighbor}} V_2(r_{ij})+\sum_{\substack{j,k\\ j\neq k}} V_3\left(\cos\theta_{ijk}\right),\end{aligned} \tag{5}$$

where the summation is for the atoms in the same unit cell, and ϕ_i is the potential energy of atom i (set V_1=0). The variables $\{r_\mathrm{b}\}$ and $\{\theta_i\}$ represent the sets of bond lengths that connect i to its neighbors and bond angles with vertex i, respectively.

2.2.2 BO potential

The BO potential is the most widely employed interatomic potential for covalent bonding systems, yet it is complicated. The functional form of the total potential for a system is

$$\Phi=\sum_{i<j}\phi_{ij}=\sum_{i<j} f_\mathrm{c}(r_{ij})\left[\phi^\mathrm{R}(r_{ij})-B_{ij}\phi^\mathrm{A}(r_{ij})\right], \tag{6}$$

where ϕ_{ij} is the interaction energy between atoms i and j, and $\phi_{ij}=\phi_{ji}$.

The interaction range of two interacting particles is determined by cutoff function $f_\mathrm{c}(r_{ij})$, and is given by

$$f_\mathrm{c}(r_{ij})=\begin{cases} 1, & r_{ij}\leq R_{ij},\\ \frac{1}{2}+\frac{1}{2}\cos\left[\frac{\pi(r_{ij}-R_{ij})}{S_{ij}-R_{ij}}\right], & R_{ij}<r_{ij}\leq S_{ij},\\ 0, & r_{ij}<S_{ij}.\end{cases} \tag{7}$$

In general, S_{ij} for covalent systems are less than the distance of the second-nearest neighbor atoms; as such, in the interaction range of these systems is the distance of the nearest neighbor.

ϕ^R and ϕ^A are pair-additive repulsive and attractive interactions, respectively, and are taken as Morse-like potentials. B_{ij} is the total BO between atoms i and j, and it allows the multi-body contributions to appear in the potential function. The functional forms of B_{ij} are various. Considering that an atom with many neighbors forms weaker bonds than an atom with fewer neighbors, Abell [41] considered ${B_{ij}}^2$ to be inversely proportional to local coordination of i and j. Tersoff [42] proposed an analytical form of B_{ij}, which is only related to bond angle (three-body interaction). Brenner [43] improved the Tersoff-type BO potential for the systems with strong π-bonding, and B_{ij} has angular and dihedral (four-body interaction) variables. In Brenner-type BO potential, B_{ij} can be written as:

$$\begin{aligned} B_{ij}&=\frac{b_{ij}+b_{ji}}{2}+F_{ij}+T_{ij},\\ b_{ij}&=\left[1+\sum_{\theta_{ijk}} f_\mathrm{c}(r_{ij})\mathrm{g}\left(\theta_{ijk}\right)\mathrm{e}^{\lambda_{ijk}}+P_{ij}\right]^{-\frac{1}{2}},\\ T_{ij}&=T_0\left[\sum_{k\neq i,j}\sum_{l\neq i,j}(1-\cos^2\varphi_{ijkl})\right],\end{aligned} \tag{8}$$

where b_{ij} and b_{ji} are covalent bonding terms, F_{ij} is a conjugation term that depends on local conjugation, and T_{ij} is a dihedral torsion term. The function $g(\theta_{ijk})$ represents the contribution of bond angles to the covalent bonding term and can be expressed as a six-order spline function. λ_{ijk} and P_{ij} are the correction factors, and the latter depends on the types of coordinating atoms. φ_{ijkl} is the dihedral torsion angle of the atomic planes ijk and ijl. Hence the potential per unit cell has the functional form:

$$\begin{aligned} \frac{\Phi}{N}&=\sum_i \phi_i\left(\{r_\mathrm{b}\},\{\cos\theta\},\{\cos\varphi\}\right),\\ \phi_i&=\frac{1}{2}\sum_j^{\text{Neighbour}} \phi_{ij}\left(r_{ij},\{\cos\theta_{ij}\},\{\cos\theta_{ji}\},\{\cos\varphi_{ij}\}\right),\end{aligned} \tag{9}$$

where $\{\theta\}$ and $\{\varphi\}$ are the sets of bond angles and dihedral torsion angles which are related to atom i. θ_{ij} is the bond angle, which is related to chemical bond i-j, where atom i is at the vertex of this angle. φ_{ij} denotes the torsion angle which is related to atoms i and j.

Before we closed this section, we need to know about the relation between the type of bonding (or bonding nature) and variables in the formulation of the aforementioned potentials for covalent systems. The bond length term is governed by the length of σ bond and is the biggest contributor to potential energy because of the high strength of the bond. In general, the bond angle term involves the relative orientation of σ bonds and the strength of π bond, while the torsion term completely depends on π bond. Given that π bonding is weak, the π bond component for angle term and the torsion term in many covalent systems are negligible.

2.3 The deformation-structural parameter relations of GL materials

In the field of nano-mechanics, developing a theory for linking the macroscopic deformation of an atomistic system to that of a continuum is crucial. The Cauchy-Born rule [44] describes the strain energy on the atomistic level for bulk materials, but it fails to extend directly to the 2-D materials [45]. Wu et al. [46] modified the Cauchy-Born rule, and developed an atomistic-based finite-deformation theory for a single-atom-thick membrane (hereafter referred to as Wu's work). The membrane should be regarded as a single smoothly curved surface in this theory, and its initial radius of curvature should be much larger than the atomic spacing. This theory can be applied to materials with the PH structure. However, this theory is not applicable for BH and 2H-MX_2 structures because the initial radius of the curvature is comparable with the atomic spacing when using the description of a single smooth curved surface for these structures. In this section, we will extend Wu's work to BH and 2H-MX_2 structures, and derive the relation between macroscopic deformation (strain and curvature) and structural parameters (bond lengths and bond angles) of the materials with PH, BH and 2H-MX_2 structures.

We will briefly introduce Wu's demonstrations about the PH structure before starting our investigations. As stated above, all atoms of an undeformed material with the PH structure lie in a plane. This plane can be curved while the system is subject to strain and curvature. Wu et al. constructed a moving frame $\{\mathbf{R}(x,y);\mathbf{T}_x,\mathbf{T}_y,\mathbf{N}\}$ on the surface, where the curvilinear coordinate system is orthogonal. Assuming that the relative position vector (RPV) of the nearest neighbor atom pair, namely, i and j, in the deformed surface denotes $\mathbf{r}_{i-j}(\Delta\xi^x,\Delta\xi^y)=\mathbf{R}(\xi_i^x,\xi_i^y)-\mathbf{R}(\xi_j^x,\xi_j^y)$, where (ξ^x,ξ^y) is the curvilinear coordinates for atoms on the deformed surface. The difference between the two coordinates can be expressed as $(\Delta\xi^x,\Delta\xi^y)=(\Delta x+r_0\eta^x,\Delta y+r_0\eta^y)$, where Δx and Δy are the difference between the two coordinates of atoms i and j on the undeformed surface (i.e., plane), and r_0 is the equilibrium bond length. $\boldsymbol{\eta}$ is the in-plane shift vector that represents the relative displacement of atoms in a unit cell and exists in non-centrosymmetric systems. When the characteristic length of deformation is much larger than the atomic spacing, $\mathbf{r}_{i-j}(\Delta\xi^x,\Delta\xi^y)$ can be expanded as follows:

$$\mathbf{r}_{i-j}(\Delta\xi^x,\Delta\xi^y)\approx\frac{\partial R}{\partial\xi^\alpha}\Delta\xi^\alpha+\frac{1}{2}\frac{\partial^2 R}{\partial\xi^\alpha\partial\xi^\beta}\Delta\xi^\alpha\Delta\xi^\beta+\frac{1}{6}\frac{\partial^3 R}{\partial\xi^\alpha\partial\xi^\beta\partial\xi^\gamma}\Delta\xi^\alpha\Delta\xi^\beta\Delta\xi^\gamma,\tag{10}$$

where $\alpha,\beta,\gamma=x,y$, and the Einstein summation convention is used. $\partial\mathbf{R}/\partial\xi^\alpha=\mathbf{T}_\alpha$ are by definition the covariant base vectors lying on the tangent surface, and has $\mathbf{T}_\alpha\cdot\mathbf{T}_\beta=\delta_{\alpha\beta}+2\varepsilon_{\alpha\beta}$. The higher order derivatives of $\mathbf{R}$ in eq. (10) are

$$\frac{\partial^2\mathbf{R}}{\partial\xi^\alpha\partial\xi^\beta}=\Gamma_{\alpha\beta}^\gamma\mathbf{T}_\gamma+\kappa_{\alpha\beta}\mathbf{N},\tag{11a}$$

and

$$\frac{\partial^3\mathbf{R}}{\partial\xi^\alpha\partial\xi^\beta\partial\xi^\gamma}=\left(\frac{\partial\Gamma_{\alpha\beta}^\nu}{\partial\gamma}-\kappa_{\alpha\beta}\kappa_{\gamma\mu}T^{\mu\nu}\right)\mathbf{T}_\nu+\Gamma_{\alpha\beta}^\nu\left(\Gamma_{\alpha\gamma}^\mu\mathbf{T}_\mu+\kappa_{\nu\gamma}\mathbf{N}\right)+\frac{\partial\kappa_{\alpha\beta}}{\partial\gamma}\mathbf{N},\tag{11b}$$

where $T^{\alpha\beta}$, $\Gamma_{\alpha\beta}^\gamma$, and $\mathbf{N}$ are the contravariant components of metric tensors for the covariant base vectors, second Christoffel symbols and the unit normal vector to the deformed surface, respectively. For infinitesimal deformation, $\Gamma_{\alpha\beta}^\gamma$ can be neglected. Thus, eq. (10) has the form:

$$\mathbf{r}_{i-j}(\Delta\xi^x,\Delta\xi^y)=\left(\Delta\xi^\alpha-\frac{1}{6}\kappa_{\beta\mu}\kappa_{\gamma\nu}T^{\nu\alpha}\Delta\xi^\beta\Delta\xi^\mu\Delta\xi^\gamma\right)\mathbf{T}_\alpha+\frac{1}{2}\kappa_{\alpha\beta}\Delta\xi^\alpha\Delta\xi^\beta\mathbf{N}+O(\kappa^3).\tag{12}$$

When the system is simultaneously subjected to strain and curvature, and then the bond length and angle of PH structure are given by

$$\begin{aligned}&r_{i-j}(\{\varepsilon\},\{\kappa\},\boldsymbol{\eta})=\sqrt{\mathbf{r}_{i-j}\cdot\mathbf{r}_{i-j}},\\&\theta_{ijk}(\{\varepsilon\},\{\kappa\},\boldsymbol{\eta})=\arccos\left(\frac{\mathbf{r}_{i-j}\cdot\mathbf{r}_{i-k}}{|\mathbf{r}_{i-j}||\mathbf{r}_{i-k}|}\right),\\&\varphi_{ijkl}(\{\varepsilon\},\{\kappa\},\boldsymbol{\eta})=\arccos\left(\frac{\mathbf{r}_{i-k}\times\mathbf{r}_{i-j}}{|\mathbf{r}_{i-k}\times\mathbf{r}_{i-j}|}\cdot\frac{\mathbf{r}_{i-j}\times\mathbf{r}_{i-l}}{|\mathbf{r}_{i-j}\times\mathbf{r}_{i-l}|}\right).\end{aligned}\tag{13}$$

Therefore, the bond length and angle are related to strain, curvature, and in-plane shift vector. However, the in-plane shift vector is not an independent variable and can be determined by minimizing the total potential energy Φ with respect to $\boldsymbol{\eta}$:

$$\frac{\partial\Phi}{\partial\boldsymbol{\eta}}=0,\tag{14a}$$

which gives:

$$\boldsymbol{\eta} = \boldsymbol{\eta}(\{\varepsilon\}, \{\kappa\}). \tag{14b}$$

Unlike the PH structure, the BH structure contains two atomic planes and the 2H-MX_2 structure contains three atomic planes. Eq. (12) is no longer applicable for these two structures because the nearest neighbor atoms are placed in different planes. Analogous to Wu's work, we consider that BH and 2H-MX_2 structures consist of three surfaces: the upper surface (S^+), the middle surface (S) and the bottom surface (S^-). S is considered as a reference surface, i.e., the strain and curvature of the materials are defined as those of S. Hence, S is the surface that is considered in the Wu's work. d^+ and d^- denote the distances between S^+ and S, and between S^- and S, respectively. We construct a moving frame $\{\mathbf{R}(x,y); \mathbf{T}_x, \mathbf{T}_y, \mathbf{N}\}$ with an orthogonal curvilinear coordinate system on S. Figure 2 illustrates S^+, S, and S^- in the deformed state.

In the case of a material with the BH structure, S^+ contains all the atoms of one of the sub-lattices, and S^- contains the rest. The height of buckling h_0 is equal to d^+ plus d^- in the equilibrium (undeformed) state, and it would be altered into $h = h_0(1+\zeta)$ in the deformed state, where ζ denotes the out-of-plane shift. We assume that atom A_1 is located in S^- and its nearest neighbor, atom B_1 is located in S^+. The points A_1' and B_1' in Figure 2(a) are the projections of A_1 and B_1 onto S. The unit normal vectors at A_1' and B_1' denote $\mathbf{N}_{A_1'}$ and $\mathbf{N}_{B_1'}$, respectively. The RPV of A_1 and B_1 is

$$\mathbf{r}_{A_1\text{-}B_1} = \mathbf{r}_{A_1'\text{-}B_1'}(\Delta\xi^x, \Delta\xi^y) + d^-\mathbf{N}_{A_1'} + d^+\mathbf{N}_{B_1'}, \tag{15}$$

where the definition of $(\Delta\xi^x, \Delta\xi^y)$ in eq. (15) are the same as that in Wu's work. For infinitesimal deformation, the form of $\mathbf{r}_{A_1'\text{-}B_1'}$ is shown in eq. (12), and $\mathbf{N}_{B_1'}$ is obtained by Taylor series expansion:

$$\mathbf{N}_{B_1'} \approx \mathbf{N}_{A_1'} + \frac{\partial \mathbf{N}_{A_1'}}{\partial \xi^\alpha}\Delta\xi^\alpha + \frac{1}{2}\frac{\partial^2 \mathbf{N}_{A_1'}}{\partial\xi^\alpha \partial\xi^\beta}\Delta\xi^\alpha\Delta\xi^\beta. \tag{16}$$

Note that the second Christoffel symbol equals zero in this case, the first- and second-order derivatives in eq. (16) are

$$\begin{aligned} \frac{\partial \mathbf{N}_{A_1'}}{\partial \xi^\alpha} &= -\kappa_{\alpha\beta}T^{\beta\gamma}\mathbf{T}_\gamma, \\ \frac{\partial^2 \mathbf{N}_{A_1'}}{\partial\xi^\alpha\partial\xi^\beta} &= -\kappa_{\alpha\gamma}\kappa_{\mu\beta}T^{\gamma\mu}\mathbf{N}. \end{aligned} \tag{17}$$

$\mathbf{N}_{B_1'}$ then becomes

$$\begin{aligned} \mathbf{N}_{B_1'} = &\left(1 - \frac{1}{2}\kappa_{\alpha\gamma}\kappa_{\mu\beta}T^{\gamma\mu}\Delta\xi^\alpha\Delta\xi^\beta\right)\mathbf{N}_{A_1'} \\ &-\kappa_{\alpha\beta}T^{\beta\gamma}\Delta\xi^\alpha\mathbf{T}_\gamma + O(\kappa^3). \end{aligned} \tag{18}$$

According to eq. (15), we have

$$\begin{aligned} \mathbf{r}_{A_1\text{-}B_1} \approx &\left(\Delta\xi^\alpha - d^+\kappa_{\beta\gamma}T^{\gamma\alpha}\Delta\xi^\beta \right. \\ &\left. -\frac{1}{6}\kappa_{\beta\mu}\kappa_{\gamma\nu}T^{\nu\alpha}\Delta\xi^\beta\Delta\xi^\mu\Delta\xi^\gamma\right)\mathbf{T}_\alpha \\ &+\left(h + \frac{1}{2}\kappa_{\alpha\beta}\Delta\xi^\alpha\Delta\xi^\beta \right. \\ &\left. -\frac{d^+}{2}\kappa_{\alpha\gamma}\kappa_{\mu\beta}T^{\gamma\mu}\Delta\xi^\alpha\Delta\xi^\beta\right)\mathbf{N}_{A_1'}. \end{aligned} \tag{19}$$

The bond length and angle are

$$\begin{aligned} r_{A_1\text{-}B_1}(\{\varepsilon\},\{\kappa\},\boldsymbol{\eta},\zeta) &= \sqrt{\mathbf{r}_{A_1\text{-}B_1}\cdot\mathbf{r}_{A_1\text{-}B_1}}, \\ \theta_{A_1B_1B_2}(\{\varepsilon\},\{\kappa\},\boldsymbol{\eta},\zeta) &= \arccos\left(\frac{\mathbf{r}_{A_1\text{-}B_1}\cdot\mathbf{r}_{A_1\text{-}B_2}}{|\mathbf{r}_{A_1\text{-}B_1}||\mathbf{r}_{A_1\text{-}B_2}|}\right). \end{aligned} \tag{20}$$

Similarly, $\boldsymbol{\eta}$ and ζ are determined by minimizing Φ, which results in

$$\boldsymbol{\eta} = \boldsymbol{\eta}(\{\varepsilon\},\{\kappa\}),\ \zeta = \zeta(\{\varepsilon\},\{\kappa\}). \tag{21}$$

For the 2H-MX_2 structure, M atoms are placed in S, and X atoms are located in S^+ and S^-. The stacking order of the three atomic planes is an ABA stacking sequence. In the equilibrium state, d^+ and d^- are identical with d_0, and they would transform $d^+ = d_0(1+\zeta^+)$ and $d^- = d_0(1+\zeta^-)$, respectively, in the deformed state. The RPV of a nearest neighbor atom pair in the 2H-MX_2 structure has the form:

$$\mathbf{r}_{M_1\text{-}X_{1'}^\pm} = \mathbf{r}_{M_1\text{-}X_{1'}^\pm}(\Delta\xi^{x\pm}, \Delta\xi^{y\pm}) \pm d^\pm\mathbf{N}_{X_{1'}^\pm}, \tag{22}$$

where $X^\pm$ denotes the X atoms in $S^\pm$, $X^{\pm\prime}$ is the projection of $X^\pm$ onto S, and $(\Delta\xi^{x\pm}, \Delta\xi^{y\pm}) = (\Delta x + a_0\eta_x^{\ \pm}, \Delta y + a_0\eta_y^{\ \pm})$ are the curvilinear coordinates for $X^\pm$ in the deformed state.

The following derivations are similar to those of the BH case. The forms of $\mathbf{r}_{M_1\text{-}X_{1'}^\pm}$ and $\mathbf{N}_{X_{1'}^\pm}$ are shown in eqs. (12) and

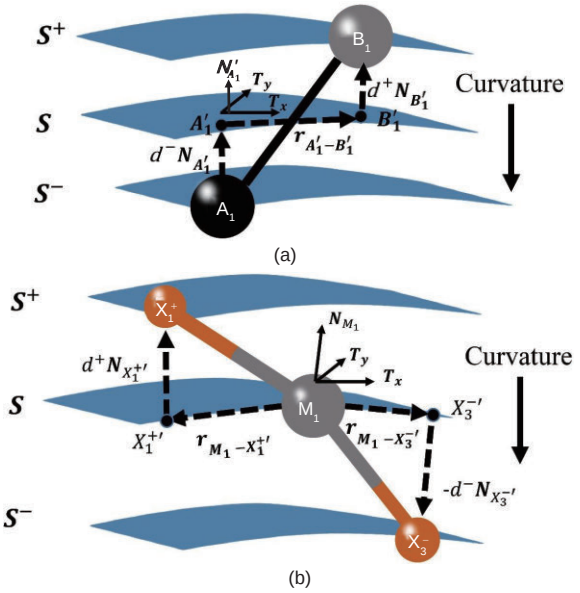

Figure 2 (Color online) Schematic representations of RPV of the nearest neighbor atom pairs of deformed (a) BH and (b) 2H-MX_2 structures. The directions of corresponding curvatures are negative (downward).

(18), respectively. Eq. (22) can be rewritten as:

$$\begin{aligned}\mathbf{r}_{\mathrm{M_1\text{-}X_1^{\pm}}} = &\left(\Delta\xi^{\alpha\pm} \mp d^{\pm}\kappa_{\beta\gamma}T^{\gamma\alpha}\Delta\xi^{\beta\pm}\right.\\ &\left.-\frac{1}{6}\kappa_{\beta\mu}\kappa_{\gamma\nu}T^{\nu\alpha}\Delta\xi^{\beta\pm}\Delta\xi^{\mu\pm}\Delta\xi^{\gamma\pm}\right)\mathbf{T}_{\alpha}\\ &+\left(\pm d^{\pm}+\frac{1}{2}\kappa_{\alpha\beta}\Delta\xi^{\alpha\pm}\Delta\xi^{\beta\pm}\right.\\ &\left.\mp\frac{d^{\pm}}{2}\kappa_{\alpha\gamma}\kappa_{\mu\beta}T^{\gamma\mu}\Delta\xi^{\alpha\pm}\Delta\xi^{\beta\pm}\right)\mathbf{N}_{\mathrm{M_1}}.\end{aligned} \tag{23}$$

The bond length and angle can be separately derived by calculating the norm of eq. (23) and the dot product of two RPVs that share the same endpoint. The in-plane shift vectors and out-of-plane shift are also related to strain and curvature:

$$\boldsymbol{\eta} = \boldsymbol{\eta}(\{\varepsilon\},\{\kappa\}),\ \ \zeta^{\pm} = \zeta^{\pm}(\{\varepsilon\},\{\kappa\}). \tag{24}$$

3 Existence criteria for GL materials

The existence criterion is constructed by a two-step deduction; for GL materials, the conditions of mechanical stability are derived from the positive definiteness of **C** and **D**. Considering the hexagonal symmetry, we obtain the set of relations:

$$\begin{aligned}&C_{11}=C_{22},\ C_{33}=2(C_{11}-C_{12}),\ C_{13}=C_{23}=0,\\ &D_{11}=D_{22},\ D_{33}=2(D_{11}-D_{12}),\ D_{13}=D_{23}=0,\end{aligned} \tag{25}$$

when the sizes of these systems are quite large and the boundary effect can be eliminated. The positive definiteness of **C** and **D** obeys the requirements:

$$\begin{aligned}&C_{11}+C_{12}>0,\quad D_{11}+D_{12}>0,\\ &C_{11}-C_{12}>0,\quad D_{11}-D_{12}>0,\end{aligned} \tag{26}$$

respectively.

The structural stability of a material with the PH structure is largely associated with the π-bonding [19,34]. In this sense, we employ BO potential to investigate the material with the PH structure. The functional form of potential per unit cell is presented in eq. (9). For PH materials, the potential can be expressed in a detailed form:

$$\begin{aligned}\frac{\Phi}{N} = &\frac{1}{2}\sum_{m=1}^{3}\left[\phi_{i_1j_m}\left(r_{i_1-j_\alpha},\left\{\cos\theta_{i_1j_m}\right\},\left\{\cos\theta_{j_mi_1}\right\},\right.\right.\\ &\left.\left\{\cos\varphi_{i_1j_m}\right\}\right)+\phi_{j_1i_m}\left(r_{j_1-i_\alpha},\left\{\cos\theta_{i_mj_1}\right\},\right.\\ &\left.\left.\left\{\cos\theta_{j_1i_m}\right\},\left\{\cos\varphi_{i_mj_1}\right\}\right)\right],\\ =&\sum_{m=1}^{3}\phi_{i_1j_m},\end{aligned} \tag{27}$$

where *i* and *j* denote two different types of atoms in a unit cell.

In the equilibrium state, all bond lengths in PH materials are equal, and all dihedral torsion angles are zero. The requirements of the extreme value condition for the potential energy with respect to r_b and φ can be expressed as follows because of lack of geometric constraint for bond length r_b and torsion angle φ,

$$\begin{aligned}&\left(\frac{\partial\phi_{ij}}{\partial r}\right)_0 = 0,\\ &\left(\frac{\partial\phi_{ij}}{\partial\varphi}\right)_0 = \left(\frac{\partial\phi_{ij}}{\partial\cos\varphi}\right)_0(-\sin\varphi)_{\varphi=0} = 0,\end{aligned} \tag{28a}$$

where the subscript "0" denotes the values in the equilibrium state. Given that $(\sin\varphi)_{\varphi=0}$ is intrinsically equal to zero, $\left(\partial\phi_{ij}/\partial\cos\varphi\right)_0$ is probably nonzero.

All equilibrium bond angles are equal to 2π/3, and they are not independent of one another. Any angle in the PH structure is geometrically equivalent to the one of the angles in $\{\theta^1,\ \theta^2,\ \theta^3\}$ and has $\sum_{\alpha=1}^{3}\theta^{\alpha}=2\pi$. However, in the viewpoint of energy, two kinds of bond angle sets exist in eq. (27): $\{\theta_i\}=\left\{\theta_i{}^1,\theta_i{}^2,\theta_i{}^3\right\}$ and $\left\{\theta_j\right\}=\left\{\theta_j{}^1,\theta_j{}^2,\theta_j{}^3\right\}$ (the angles are shown in Figure 1(a)). The summation of the element of each kind is also equal to 2π. Using Lagrange conditional extremum theory, we obtain

$$\begin{aligned}&\frac{\partial\Phi}{\partial\theta_i^1}=\frac{\partial\Phi}{\partial\theta_i^2}=\frac{\partial\Phi}{\partial\theta_i^3}=\lambda_i,\\ &\frac{\partial\Phi}{\partial\theta_j^1}=\frac{\partial\Phi}{\partial\theta_j^2}=\frac{\partial\Phi}{\partial\theta_j^3}=\lambda_j,\end{aligned} \tag{28b}$$

where λ_i and λ_j are Lagrange multipliers. In accordance with the constraints, these multipliers can be calculated by solving eq. (28b). Generally, λ_i and λ_j are not the same because the contributions to the potential energy for each kind of bond angles are different, except for the same types of atoms *i* and *j*. As eq. (28b) yields

$$\begin{aligned}&\left(\frac{\partial\phi_{ij}}{\partial\cos\theta_i}\right)_0 = -\frac{\sqrt{3}}{3}\lambda_i,\\ &\left(\frac{\partial\phi_{ij}}{\partial\cos\theta_j}\right)_0 = -\frac{\sqrt{3}}{3}\lambda_j,\end{aligned} \tag{28c}$$

the values of $\left(\partial\phi_{ij}/\partial\cos\theta_i\right)_0$ and $\left(\partial\phi_{ij}/\partial\cos\theta_j\right)_0$ are nonzero and different.

Eq. (28) indicates the extreme value conditions of Φ for PH materials. The structural parameters of the materials are determined by solving such equations.

The subsequent step is deriving the conditions of mechanical stability for PH materials. According to the analytical form of BO potential (eqs. (27) and (28)), the elements of **C** and **D** can be expanded as follows:

$$\frac{\Phi_{e_{\alpha\beta},e_{\gamma\delta}}}{N}=\sum_{m=1}^{3}\Bigg\{\frac{\partial^2\phi_{ij}}{\partial r^2}\frac{\partial r_{i_1-j_m}}{\partial e_{\alpha\beta}}\frac{\partial r_{i_1-j_m}}{\partial e_{\gamma\delta}}+\sum_{\varphi=\left\{\varphi_{i_1j_m}\right\}}\frac{\partial\phi_{ij}}{\partial\cos\varphi}\frac{\partial^2\cos\varphi}{\partial e_{\alpha\beta}\partial e_{\gamma\delta}}+\sum_{\varphi=\left\{\varphi_{i_1j_m}\right\}}\Bigg[\frac{\partial^2\phi_{ij}}{\partial\cos\varphi^2}\frac{\partial\cos\varphi}{\partial e_{\alpha\beta}}\frac{\partial\cos\varphi}{\partial e_{\gamma\delta}}+\frac{\partial^2\phi_{ij}}{\partial r\partial\cos\varphi}\left(\frac{\partial r_{i_1-j_m}}{\partial e_{\alpha\beta}}\frac{\partial\cos\varphi}{\partial e_{\gamma\delta}}+\frac{\partial r_{i_1-j_m}}{\partial e_{\gamma\delta}}\frac{\partial\cos\varphi}{\partial e_{\alpha\beta}}\right)\Bigg]+2\sum_{\theta=\left\{\theta_{i_1j_m}\right\}}\Bigg[\frac{\partial\phi_{ij}}{\partial\cos\theta}\frac{\partial^2\cos\theta}{\partial e_{\alpha\beta}\partial e_{\gamma\delta}}+\frac{\partial^2\phi_{ij}}{\partial r\partial\cos\theta}\left(\frac{\partial r_{i_1-j_m}}{\partial e_{\alpha\beta}}\frac{\partial\cos\theta}{\partial e_{\gamma\delta}}+\frac{\partial r_{i_1-j_m}}{\partial e_{\gamma\delta}}\frac{\partial\cos\theta}{\partial e_{\alpha\beta}}\right)\Bigg]+2\sum_{\theta\neq\theta';\theta,\theta'=\left\{\theta_{i_1j_m}\right\}}\frac{\partial^2\phi_{ij}}{\partial\cos\theta\partial\cos\theta'}\times\frac{\partial\cos\theta}{\partial e_{\alpha\beta}}\frac{\partial\cos\theta}{\partial e_{\gamma\delta}}\Bigg\}_0, \tag{29}$$

where we define

$$\frac{\partial\phi_{ij}}{\partial\cos\theta}=\frac{1}{2}\left(\frac{\partial\phi_{ij}}{\partial\cos\theta_i}+\frac{\partial\phi_{ij}}{\partial\cos\theta_j}\right),$$
$$\frac{\partial^2\phi_{ij}}{\partial r\partial\cos\theta}=\frac{1}{2}\left(\frac{\partial^2\phi_{ij}}{\partial r\partial\cos\theta_i}+\frac{\partial^2\phi_{ij}}{\partial r\partial\cos\theta_j}\right), \tag{30}$$
$$\frac{\partial^2\phi_{ij}}{\partial\cos\theta\partial\cos\theta'}=\frac{1}{2}\left(\frac{\partial^2\phi_{ij}}{\partial\cos\theta_i\partial\cos\theta_i'}+\frac{\partial^2\phi_{ij}}{\partial\cos\theta_j\partial\cos\theta_j'}\right).$$

The deformation-structural parameter relations for PH materials are presented in eqs. (12) and (13), where the in-plane shift vector has the form:

$$\eta_x=\frac{1}{2}F(\varepsilon_{xx}-\varepsilon_{yy}),$$
$$\eta_y=-F\varepsilon_{xy}, \tag{31}$$

where the derivation process and analytical expression of F are shown in Appendix. By substituting eqs. (12), (13), and (31) into eq. (29), the elements of **C** and **D** are derived, and their analytical expressions are available in eqs. (a3) and (a4). Table 1 presents the results for PH materials, which have been successfully synthesized, except for SiC. Obviously, the conditions in eq. (26) are satisfied for the BH materials in Table 1.

The strength of π-bonding in BH materials is generally weak. In other words, the four-body interaction and high order interactions in these systems are negligible. For simplicity, SW potential is used. The potential per unit cell for a BH material is

Table 1 The structural parameters and numerical values of elements of **C** and **D** for PH materials

PH materials	a_0 (Å)	C_{11} (eV)	C_{12} (eV)	D_{11} (eV Å^2)	D_{12} (eV Å^2)
C [42]	1.42	94.36	37.48	11.08	2.55
BN [47]	1.44	93.43	29.06	10.79	3.87
SiC [48]	1.82	95.78	18.79	4.68	4.55
GaN [49]	1.93	67.31	36.62	0.23	0.19

$$\frac{\Phi}{N}=\sum_{m=1}^{3}V_2(r_{\mathrm{A}_1-\mathrm{B}_m})+\sum_{\substack{m,n=1\\m>n}}^{3}\left[V_3\left(\cos\theta_{\mathrm{A}_1\mathrm{B}_m\mathrm{B}_n}\right)+V_3\left(\cos\theta_{\mathrm{B}_1\mathrm{A}_m\mathrm{A}_n}\right)\right]. \tag{32}$$

Given the lack of geometric constraints for bond length r_b and height of buckling h, we have the extreme value conditions:

$$\left(\frac{\partial V_2}{\partial r}\right)_0=0,$$
$$\frac{h_0}{r_0}\left(\frac{\partial V_2}{\partial r}\right)_0+\frac{3h_0{a_0}^2}{{r_0}^4}\left(\frac{\partial V_3}{\partial\cos\theta_\mathrm{A}}+\frac{\partial V_3}{\partial\cos\theta_\mathrm{B}}\right)_0=0. \tag{33a}$$

Two independent conditions respectively make the second equation in eq. (33a) true: $h_0=0$ and $\left(\partial V_3/\partial\cos\theta_\mathrm{A}+\partial V_3/\partial\cos\theta_\mathrm{B}\right)_0=0$. The former corresponds to the case of materials with the PH structure. For BP materials, the latter condition must be met. According to the analytical form of SW potential, the sign of $\left(\partial V_3/\partial\cos\theta_\mathrm{A}\right)_0$ is generally the same with that of $\left(\partial V_3/\partial\cos\theta_\mathrm{B}\right)_0$. Hence, the second equation in eq. (33a) gives

$$\left(\frac{\partial V_3}{\partial\cos\theta_\mathrm{A}}\right)_0=\left(\frac{\partial V_3}{\partial\cos\theta_\mathrm{B}}\right)_0=0. \tag{33b}$$

According to eqs. (32) and (33), the elements of **C** and **D** have the forms:

$$\frac{\Phi_{e_{\alpha\beta},e_{\gamma\delta}}}{N}=\sum_{m=1}^{3}\frac{\partial^2V_2}{\partial r^2}\frac{\partial r_{\mathrm{A}_1\text{-}\mathrm{B}_m}}{\partial e_{\alpha\beta}}\frac{\partial r_{\mathrm{A}_1\text{-}\mathrm{B}_m}}{\partial e_{\gamma\delta}}+\sum_{\substack{m,n=1\\m>n}}^{3}\frac{\partial^2V_3}{\partial\cos\theta_\mathrm{A}{}^2}\frac{\partial\cos\theta_{\mathrm{A}_1\mathrm{B}_m\mathrm{B}_n}}{\partial e_{\alpha\beta}}\frac{\partial\cos\theta_{\mathrm{A}_1\mathrm{B}_m\mathrm{B}_n}}{\partial e_{\gamma\delta}}+\sum_{\substack{m,n=1\\m>n}}^{3}\frac{\partial^2V_3}{\partial\cos\theta_\mathrm{B}{}^2}\frac{\partial\cos\theta_{B_1A_mA_n}}{\partial e_{\alpha\beta}}\frac{\partial\cos\theta_{B_1A_mA_n}}{\partial e_{\gamma\delta}}. \tag{34}$$

Eqs. (19) and (20) show the deformation-structural parameter relations for BH materials. The shift vector has the form:

$$\eta_x = \frac{1}{2}G(\varepsilon_{xx} - \varepsilon_{yy}),$$
$$\eta_y = -G\varepsilon_{xy}, \tag{35}$$
$$\zeta = H\left(\varepsilon_{xx} + \varepsilon_{yy}\right).$$

The analytical expressions of G, H and elements of **C** and **D** are shown in eqs. (a9)-(a13). The results for the BH materials, which have been proved to be stable by experimental studies and theoretical derivations, are provided in Table 2. The conditions in eq. (26) are satisfied for the BH materials in Table 2.

In the case of a material with the 2H-MX_2 structure, we also employ SW potential. The potential energy per unit cell has the form:

$$\begin{aligned}\frac{\Phi}{N} = &\sum_{n=1}^{3}\sum_{\sigma=\pm} V_2(r_{\mathrm{M_1\text{-}X_n^\sigma}}) \\ &+ \sum_{\substack{m,n=1\\ m>n}}^{3}\sum_{\sigma=\pm} V_3\left(\cos\theta_{\mathrm{M_1X_n^\sigma X_m^\sigma}}\right) \\ &+ \sum_{n=1}^{3}\sum_{\substack{\sigma',\sigma=\pm\\ \sigma'\neq\sigma}} V_3\left(\cos\theta_{\mathrm{M_1X_n^\sigma X_n^{\sigma'}}}\right) \\ &+ \sum_{\substack{m,n=1\\ m>n}}^{3}\sum_{\sigma=\pm} V_3\left(\cos\theta_{\mathrm{X_n^\sigma M_n M_m}}\right).\end{aligned} \tag{36}$$

Similarly, given the lack of geometric constraints for bond length r_b and interlayer distance h, the extreme value conditions are

$$\begin{aligned}&\left(\frac{\partial V_2}{\partial r}\right)_0 = 0, \\ &\left(\frac{\partial V_3}{\partial \cos\theta_{\mathrm{M_1X_n^\sigma X_m^\sigma}}}\right)_0 = \left(\frac{\partial V_3}{\partial \cos\theta_{\mathrm{M_1X_n^\sigma X_n^{\sigma'}}}}\right)_0 \\ &\qquad = \left(\frac{\partial V_3}{\partial \cos\theta_{\mathrm{X_n^\sigma M_n M_m}}}\right)_0 = 0.\end{aligned} \tag{37}$$

Table 2 The structural parameters and numerical values of elements of **C** and **D** for BH materials. The parameters of interatomic potentials are acquired from ref. [39]

BH materials	a_0 (Å)	h_0 (Å)	C_{11} (eV)	C_{12} (eV)	D_{11} (eV Å^2)	D_{12} (eV Å^2)
Si	2.23	0.45	53.31	8.08	8.12	2.71
Ge	2.34	0.69	49.97	9.34	16.55	5.52
Sn	2.70	0.86	21.96	5.54	9.75	3.25
SiGe	2.25	0.54	46.25	7.48	9.97	3.32
SnSi	2.43	0.67	38.59	5.44	13.23	4.41
InP	2.41	0.51	38.26	6.69	6.98	2.33
InAs	2.47	0.63	35.43	6.08	10.12	3.37
InSb	2.64	0.74	33.82	5.73	13.37	4.46
GaAs	2.29	0.56	44.81	5.78	11.29	3.76
GaP	2.22	0.38	44.59	5.32	5.36	1.79
AlSb	2.50	0.60	44.14	6.74	11.82	3.94

According to eqs. (36) and (37), the elements of **C** and **D** can be expressed as:

$$\begin{aligned}\frac{\Phi_{e_{\alpha\beta},e_{\gamma\delta}}}{N} = &\sum_{n=1}^{3}\sum_{\sigma=\pm}\left(\frac{\partial^2 V_2}{\partial r^2}\right)\frac{\partial r_{\mathrm{M_1\text{-}X_n^\sigma}}}{\partial e_{\alpha\beta}}\frac{\partial r_{\mathrm{M_1\text{-}X_n^\sigma}}}{\partial e_{\gamma\delta}} \\ &+ \sum_{\substack{m,n=1\\ m>n}}^{3}\sum_{\sigma=\pm}\left(\frac{\partial^2 V_3}{\partial \cos\theta_{\mathrm{M_1X_n^\sigma X_m^\sigma}}^2}\right) \\ &\times\frac{\partial\cos\theta_{\mathrm{M_1X_n^\sigma X_m}}}{\partial e_{\alpha\beta}}\frac{\partial\cos\theta_{\mathrm{M_1X_n^\sigma X_m}}}{\partial e_{\gamma\delta}} \\ &+ \sum_{n=1}^{3}\sum_{\substack{\sigma',\sigma=\pm\\ \sigma'\neq\sigma}}\left(\frac{\partial^2 V_3}{\partial \cos\theta_{\mathrm{M_1X_n^\sigma X_n^{\sigma'}}}^2}\right) \\ &\times\frac{\partial\cos\theta_{\mathrm{M_1X_n^\sigma X_n^{\sigma'}}}}{\partial e_{\alpha\beta}}\frac{\partial\cos\theta_{\mathrm{M_1X_n^\sigma X_n^{\sigma'}}}}{\partial e_{\gamma\delta}} \\ &+ \sum_{\substack{m,n=1\\ m>n}}^{3}\sum_{\sigma=\pm}\left(\frac{\partial^2 V_3}{\partial \cos\theta_{\mathrm{X_1^\sigma M_n M_m}}^2}\right) \\ &\times\frac{\partial\cos\theta_{\mathrm{X_1^\sigma M_n M_m}}}{\partial e_{\alpha\beta}}\frac{\partial\cos\theta_{\mathrm{X_1^\sigma M_n M_m}}}{\partial e_{\gamma\delta}}.\end{aligned} \tag{38}$$

Eq. (25) shows the deformation-structural parameter relations for 2H-MX_2 materials. The shift vector has the form:

$$\eta_x^{\pm} = \frac{1}{2}I(\varepsilon_{xx} - \varepsilon_{yy}) \pm \frac{1}{2}J(\kappa_{xx} - \kappa_{yy}),$$
$$\eta_y^{\pm} = -I\varepsilon_{xy} \mp J\kappa_{xy}, \tag{39}$$
$$\zeta^{\pm} = L\left(\varepsilon_{xx} + \varepsilon_{yy}\right) \pm N\left(\kappa_{xx} + \kappa_{yy}\right).$$

The analytical expressions of I, J, L, M and elements of **C** and **D** are given in eqs. (a21)-(a31). The results for the 2H-MX_2 materials that were successfully synthesized in the laboratory are reported in Table 3. Clearly, the conditions in eq. (26) are met for the 2H-MX_2 materials in Table 3.

The out-of-plane deformation is a new nano-mechanical phenomenon [32]. Hence, we believe that **D** shows the leading feature of stability of low-dimensional materials. The matrix **D** for PH and BH materials is irrelevant to the derivative of the interatomic potential with respect to the bond length (eqs. (a4) and (a13)). Given that this derivative represents the strength of σ bond, BH and PH materials may exhibit low ability to resist out-of-plane perturbation; as such, their existence criteria are somehow draconian (eqs. (a7) and (a19)). For 2H-MX_2 materials, however, the analytical expression of matrix **D** possesses the bond length-related derivative (eq. (a31)), indicating that this matrix contains more contributions of σ bond. Such materials have relatively high bending capacity, and meet the requirements of their existence criteria is not difficult. Hence, BH and PH materials are sometimes difficult to be isolated or synthesized in the laboratory; by contrast, 2H-MX_2 materials can be easily exfoliated from their bulk materials.

Table 3 The structural parameters and numerical values of elements of **C** and **D** for BH materials. The parameters of interatomic potentials are acquired from ref. [39]

BH materials	a_0 (Å)	d_0 (Å)	C_{11} (eV)	C_{12} (eV)	D_{11} (eV Å^2)	D_{12} (eV Å^2)
MoS_2	1.80	1.60	55.39	14.87	73.62	19.50
$MoSe_2$	1.92	1.65	65.34	15.35	104.69	26.39
$MoTe_2$	2.05	1.80	57.97	14.31	108.97	27.89
WS_2	1.81	1.56	68.31	14.43	99.07	24.83
WSe_2	1.88	1.67	74.18	14.60	123.19	30.70
NbS_2	1.91	1.56	56.52	15.22	73.32	19.66
$NbSe_2$	1.99	1.67	57.05	16.58	90.93	23.37
TaS_2	1.91	1.58	56.36	15.32	74.01	19.89
$TaSe_2$	1.98	1.67	57.10	16.70	81.20	22.18

4 The validity of plate models for GL materials

According to classical linear-elastic plate theory, the relation between elastic constant matrix at the plane-stress condition and bending stiffness matrix is [50]

$$\mathbf{D}_{\mathrm{P}} = \frac{h_{\mathrm{P}}^3}{12}\mathbf{C}_{\mathrm{P}}, \tag{40}$$

where h_{P} is the thickness of the plate. Assuming the presence of universal constant effective thickness h_{eff}, by definition of **C** and **D** in this paper, we have

$$\mathbf{C}_{\mathrm{P}} = \frac{\mathbf{C}}{Sh_{\mathrm{eff}}}, \quad \mathbf{D}_{\mathrm{P}} = \frac{\mathbf{D}}{S}, \tag{41}$$

where S is the area of a unit cell in a 2-D material. If the 2-D system under arbitrary loadings can be idealized as a linear-elastic plate, $\mathbf{C}_{\mathrm{P}}$ and $\mathbf{D}_{\mathrm{P}}$ in eq. (41) must satisfy eq. (40). In other words, as long as the multiple relationships between **C** and **D** are met, classical thin plate models are applicable to 2-D materials. Otherwise, a universal constant thickness cannot be defined, and the effective thickness depends on the type of loading [30]. For instance, when the 2-D material is subjected to uniaxial bending (e.g., $\kappa_{yy} = \kappa_{xy} = 0$), the effective thickness is $h_{\mathrm{eff}}^{11} = \sqrt{12D_{11}/C_{11}}$; for torsion ($\kappa_{xx} = \kappa_{yy} = 0$) the thickness becomes $h_{\mathrm{eff}}^{33} = \sqrt{12D_{33}/C_{33}}$. If the multiple relationships between **C** and **D** are violated, then h_{eff}^{11} may not be equal to h_{eff}^{33}. As a result, according to eq. (25), when

$$\frac{C_{11}}{C_{12}} = \frac{D_{11}}{D_{12}}, \tag{42}$$

the GL material under arbitrary loadings can be modeled as an isotropic thin plate.

For the materials in Tables 1-3, eq. (42) is not rigorously satisfied. As such, these materials cannot be strictly idealized as thin plates. Here we define a factor of validity:

$$t = \frac{\mathrm{Min}(C_{11}/C_{12}, D_{11}/D_{12})}{\mathrm{Max}(C_{11}/C_{12}, D_{11}/D_{12})} \times 100\%, \tag{43}$$

which represents the validity of using thin plate models to investigate the overall mechanical response of GL sheets. An extreme case of t = 100% means that the 2-D sheet can be completely regarded as a classical thin plate.

The results for the GL materials discussed in the previous section are presented in Figure 3. Among these materials, single-layer NbS_2 has the highest value of t = 99.5% which is very close to 100%. PH SiC has the lowest t = 20.2%, and it results in highly scattered values of effective thickness. Thus the phenomenon of so called ''Yakobson's paradox'' [31] is evident for this material.

As shown in Figure 3, factors t (the percentages in Figure 3) for the materials with 2H-MX_2 structure is higher than those for PH and BH materials on the whole. This result can be attributed to the three-atom-thick nature of 2H-MX_2 structure. When the 2H-MX_2 material is subjected to a positive curvature, the length of the chemical bond that connects M to X^+ ($r_{\mathrm{M\text{-}X^+}}$) is shortened, while $r_{\mathrm{M\text{-}X^-}}$ is elongated. This behavior is analogous to the strain response of classical thin plate under pure bending distortion. On the other hand, asymmetric tensile and compressive strains on the different sides of the natural surface of thin plates are on the order of κ. The change in the element length of the plate along the principal curvature is also on the order of κ, unless the element is located on the natural surface. For a bent 2H-MX_2 sheet, the change in the bond length is $\Delta r_{\mathrm{b}} \sim \kappa$, while for bent PH and BH sheets, the length is $\Delta r_{\mathrm{b}} \sim \kappa^2$. Moreover, in the viewpoint of the bonding nature, the breakdown of thin plate theory for single-atom-thick sheet is caused by the lack of σ bond participation while the sheet is bending [32]. As mentioned above, the changes in the length and relative orientation of σ bonds in the bent 2H-MX_2 sheet are larger than those in the bent PH and BH sheets. In contrast to PH and BH sheets, the structural response of 2H-MX_2 for arbitrary loading sheet closely resembles that of classical thin plate.

Given the single-atom-thick nature, the bending behavior of PH materials significantly differs from that of classic thin plate. According to eqs. (a3) and (a4), the bending resistance for PH materials is mainly related to π bonding (note the

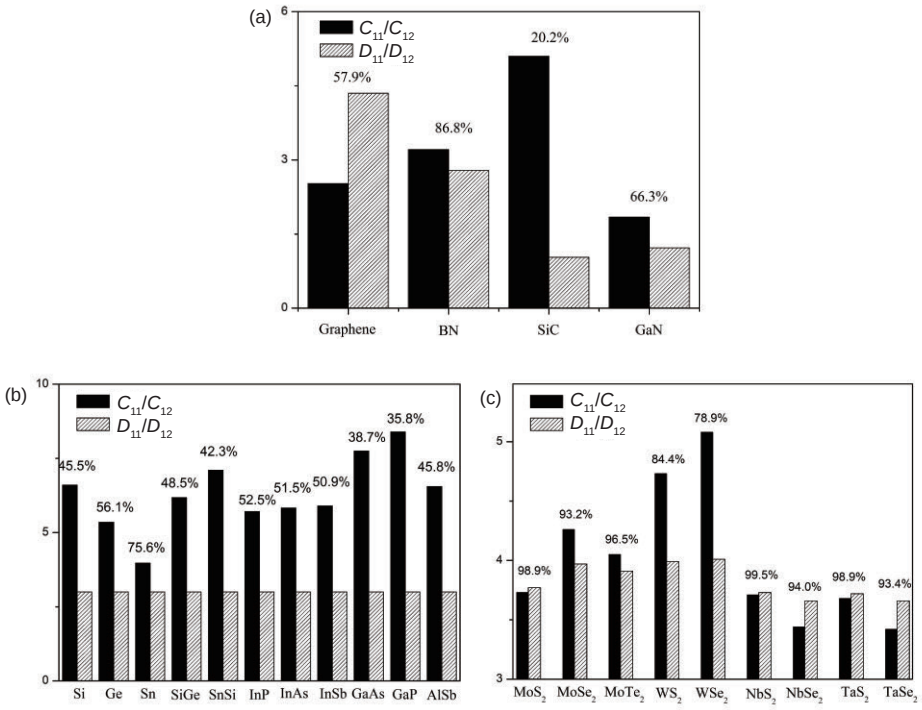

Figure 3 The factors of validity (expressed as percentages), C_{11}/C_{12}, and D_{11}/D_{12}, for (a) PH, (b) BH, (c) 2H-MX_2 materials.

value of $\left(\partial\phi_{ij}/\partial\cos\varphi\right)_0$ completely depends on the strength of π bond). For thin plates, the bending resistance originates from σ-bond distortion. Therefore, the relatively low value of t of PH materials is not surprising.

A bent BH material involves extension and compression on different sides of S because the material has an atomic-scale out-of-plane buckling. Intuitively, BH material has a higher applicability of classical thin plate models than PH material. As shown in Figure 3(a) and (b), the value of t is not significantly different between these two kinds of GL materials. This finding can be explained as follows. Given that the BO potential employed does not contain long-range interaction (it is valid for most covalent bonding systems), the atoms of BH materials in the same atomic plane are not interacting even the systems are stretched or bent. That is, the potential energy of BH materials has nothing to do with in-plane atomic interaction. Nevertheless, for a classic plate with macroscopic thickness, the bending strain energy is dominated by in-plane strain on each layer. Such differences in the generation of strain energy lead to the breakdown of thin plate models in the BH materials.

5 Concluding remarks

We have used an atomistic potential-based approach to establish the existence criteria for PH, BH and 2H-MX_2 materials. We also discuss the validity of plate idealization for these materials. The deformation-structural parameter relations for two- and three-atom layered structures were constructed to acquire analytical expressions of the criteria. In contrast to PH and BH materials, 2H-MX_2 materials can easily exist in isolation as σ bond strengthens their bending capacity. The validity of the thin plate models was investigated by analyzing the multiple relations between **C** and **D**, whose elements are the quadratic terms of the potential energy. To facilitate the analysis, we propose a factor of validity to examine the validity of plate idealization. The results show that all of the three kinds of GL materials under arbitrary loadings cannot be strictly idealized as thin plates. Nevertheless, the plate idealization of 2H-MX_2 sheets may be appropriate because their structural response is analogous to that of thin plates for arbitrary loadings. Moreover, although the BH materials investigated possess multi-layered nature, they cannot be modeled as thin plates due to the weakness of long-range interaction for covalent bonding systems. The approach and analysis in this paper are applicable to other 2-D materials, such phosphorene [51]. Therefore, the results are valuable in understanding and developing mechanics of 2-D materials.

This work was supported by the National Natural Science Foundation of China (Grant Nos. 11832019, 11472313, and 11572355). The authors would like to thank Dr. Yangfan Hu and Dr. Baofu Zhang for the useful advices.

1 K. S. Novoselov, A. K. Geim, S. V. Morozov, D. Jiang, Y. Zhang, S. V. Dubonos, I. V. Grigorieva, and A. A. Firsov, Science **306**, 666 (2004).
2 K. S. Novoselov, Rev. Mod. Phys. **83**, 837 (2011).
3 P. R. Wallace, Phys. Rev. **71**, 622 (1947).

4 M. Xu, T. Liang, M. Shi, and H. Chen, Chem. Rev. **113**, 3766 (2013).
5 B. Feng, Z. Ding, S. Meng, Y. Yao, X. He, P. Cheng, L. Chen, and K. Wu, Nano Lett. **12**, 3507 (2012), arXiv: 1203.2745.
6 N. Alem, R. Erni, C. Kisielowski, M. D. Rossell, W. Gannett, and A. Zettl, Phys. Rev. B **80**, 155425 (2009).
7 S. Manzeli, D. Ovchinnikov, D. Pasquier, O. V. Yazyev, and A. Kis, Nat. Rev. Mater. **2**, 17033 (2017).
8 L. Li, S. Lu, J. Pan, Z. Qin, Y. Wang, Y. Wang, G. Cao, S. Du, and H. J. Gao, Adv. Mater. **26**, 4820 (2014).
9 F. F. Zhu, W. J. Chen, Y. Xu, C. L. Gao, D. D. Guan, C. H. Liu, D. Qian, S. C. Zhang, and J. F. Jia, Nat. Mater. **14**, 1020 (2015), arXiv: 1506.01601.
10 P. Joensen, R. F. Frindt, and S. R. Morrison, Mater. Res. Bull. **21**, 457 (1986).
11 X. Wang, Y. Gong, G. Shi, W. L. Chow, K. Keyshar, G. Ye, R. Vajtai, J. Lou, Z. Liu, E. Ringe, B. K. Tay, and P. M. Ajayan, ACS Nano **8**, 5125 (2014).
12 J. Chen, B. Liu, Y. Liu, W. Tang, C. T. Nai, L. Li, J. Zheng, L. Gao, Y. Zheng, H. S. Shin, H. Y. Jeong, and K. P. Loh, Adv. Mater. **27**, 6722 (2015).
13 M. Hafeez, L. Gan, H. Li, Y. Ma, and T. Zhai, Adv. Mater. **28**, 8296 (2016).
14 P. Miró, M. Audiffred, and T. Heine, Chem. Soc. Rev. **43**, 6537 (2014).
15 C. R. Dean, A. F. Young, I. Meric, C. Lee, L. Wang, S. Sorgenfrei, K. Watanabe, T. Taniguchi, P. Kim, K. L. Shepard, and J. Hone, Nat. Nanotech. **5**, 722 (2010), arXiv: 1005.4917.
16 B. Radisavljevic, M. B. Whitwick, and A. Kis, ACS Nano **5**, 9934 (2011).
17 Q. Peng, J. Crean, A. K. Dearden, C. Huang, X. Wen, S. P. A. Bordas, and S. De, Mod. Phys. Lett. B **27**, 1330017 (2013).
18 A. Pakdel, Y. Bando, and D. Golberg, Chem. Soc. Rev. **43**, 934 (2014).
19 H. Şahin, S. Cahangirov, M. Topsakal, E. Bekaroglu, E. Akturk, R. T. Senger, and S. Ciraci, Phys. Rev. B **80**, 155453 (2009), arXiv: 0907.4350.
20 K. A. N. Duerloo, Y. Li, and E. J. Reed, Nat. Commun. **5**, 4214 (2014).
21 Z. P. Xu, and Q. S. Zheng, Sci. China-Phys. Mech. Astron. **61**, 074601 (2018).
22 W. Yang, H. T. Wang, T. F. Li, and S. X. Qu, Sci. China-Phys. Mech. Astron. **62**, 14601 (2019).
23 K. N. Kudin, G. E. Scuseria, and B. I. Yakobson, Phys. Rev. B **64**, 235406 (2001).
24 S. Kitipornchai, X. Q. He, and K. M. Liew, Phys. Rev. B **72**, 075443 (2005).
25 J. Peng, J. Wu, K. C. Hwang, J. Song, and Y. Huang, J. Mech. Phys. Solids **56**, 2213 (2008).
26 M. M. Shokrieh, and R. Rafiee, Mater. Des. **31**, 790 (2010).
27 Y. Liu, Z. Xu, and Q. Zheng, J. Mech. Phys. Solids **59**, 1613 (2011).
28 A. Genoese, A. Genoese, N. L. Rizzi, and G. Salerno, Compos. Part B-Eng. **115**, 316 (2017).
29 Z. Q. Wang, and Y. P. Zhao, Sci. China-Phys. Mech. Astron. **54**, 948 (2011).
30 Y. Huang, J. Wu, and K. C. Hwang, Phys. Rev. B **74**, 245413 (2006).
31 O. A. Shenderova, V. V. Zhirnov, and D. W. Brenner, Critical Rev. Solid State Mater. Sci. **27**, 227 (2002).
32 D. B. Zhang, E. Akatyeva, and T. Dumitrică, Phys. Rev. Lett. **106**, 255503 (2011).
33 E. Gao, and Z. Xu, J. Appl. Mech **82**, 121012 (2015).
34 J. Chen, B. Wang, and Y. Hu, J. Mech. Phys. Solids **107**, 451 (2017), arXiv: 1610.01467.
35 M. Born, Math. Proc. Camb. Phil. Soc. **36**, 160 (1940).
36 Y. C. Fung, *Foundations of Solid Mechanics* (Prentice Hall, Englewood, 1965), pp. 341-359.
37 M. S. Daw, and M. I. Baskes, Phys. Rev. B **29**, 6443 (1984).
38 F. H. Stillinger, and T. A. Weber, Phys. Rev. B **31**, 5262 (1985).
39 J. A. Harrison, M. Fallet, K. E. Ryan, B. L. Mooney, M. T. Knippenberg, and J. D. Schall, Model. Simul. Mater. Sci. Eng. **23**, 074003 (2015).
40 J. Jiang, and Y. Zhou, *Handbook of Stillinger-Weber Potential Parameters for Two-Dimensional Atomic Crystals* (IntechOpen, Londo, 2017).
41 G. C. Abell, Phys. Rev. B **31**, 6184 (1985).
42 J. Tersoff, Phys. Rev. Lett. **56**, 632 (1986).
43 D. W. Brenner, O. A. Shenderova, J. A. Harrison, S. J. Stuart, B. Ni, and S. B. Sinnott, J. Phys.-Condens. Matter **14**, 783 (2002).
44 M. Born, and K. Huang, *Dynamical Theory of Crystal Lattices* (Oxford University Press, Oxford, 1959), pp. 120-139.
45 M. Arroyo, and T. Belytschko, J. Mech. Phys. Solids **50**, 1941 (2002).
46 J. Wu, K. C. Hwang, and Y. Huang, J. Mech. Phys. Solids **56**, 279 (2008).
47 C. Sevik, A. Kinaci, J. B. Haskins, and T. Çağın, Phys. Rev. B **84**, 085409 (2011).
48 P. Erhart, and K. Albe, Phys. Rev. B **71**, 035211 (2005).
49 J. Nord, K. Albe, P. Erhart, and K. Nordlund, J. Phys.-Condens. Matter **15**, 5649 (2003).
50 E. Ventsel, and T. Krauthammer, *Thin Plates and Shells* (Marcel Dekker, New York, 2001), pp. 17-23.
51 H. Liu, A. T. Neal, Z. Zhu, Z. Luo, X. Xu, D. Tománek, and P. D. Ye, ACS Nano **8**, 4033 (2014).

Appendix Analytical expressions of shift vector and elements of C and D for PH, BH and 2H-MX_2 materials

As mentioned in sect. 2.3, the shift vector $\boldsymbol{\eta}$ is determined by solving eq. (14a). In the case of PH materials, these equations can be expanded as:

$$\frac{\partial \Phi}{\partial \eta_\gamma} = \sum_{\alpha,\beta}\left(\frac{\partial^2 \Phi}{\partial \varepsilon_{\alpha\beta}\partial \eta_\gamma}\varepsilon_{\alpha\beta} + \frac{\partial^2 \Phi}{\partial \kappa_{\alpha\beta}\partial \eta_\gamma}\kappa_{\alpha\beta}\right) + \sum_{\alpha}\frac{\partial^2 \Phi}{\partial \eta_\alpha \partial \eta_\gamma}\eta_\alpha = 0, \tag{a1}$$

with respect to infinitesimal deformation, where $\alpha, \beta, \gamma = x, y$. Eq. (a1) yields eq. (31) without considering boundary effect, and analytical expression of F in eq. (31) is

$$F = \frac{12\left(\frac{\partial \phi_{ij}}{\partial \cos\theta}\right)_0 + 18\left(\frac{\partial^2 \phi_{ij}}{\partial \cos\theta^2}\right)_{\theta=\frac{2\pi}{3}} - 9\left(\frac{\partial^2 \phi_{ij}}{\partial \cos\theta \partial \cos\theta'}\right)_0 - 2r_0{}^2\left(\frac{\partial^2 \phi_{ij}}{\partial r^2}\right)_0}{12\left(\frac{\partial \phi_{ij}}{\partial \cos\theta}\right)_0 + 18\left(\frac{\partial^2 \phi_{ij}}{\partial \cos\theta^2}\right)_{\theta=\frac{2\pi}{3}} - 9\left(\frac{\partial^2 \phi_{ij}}{\partial \cos\theta \partial \cos\theta'}\right)_0 + 12r_0\left(\frac{\partial^2 \phi_{ij}}{\partial r \partial \cos\theta}\right)_0 + 2r_0{}^2\left(\frac{\partial^2 \phi_{ij}}{\partial r^2}\right)_0}. \tag{a2}$$

The elements of **C** and **D** are

$$C_{11}=C_{22}=\frac{9}{8}{r_0}^2\left(\frac{\partial^2\phi_{ij}}{\partial r^2}\right)_0+\frac{1}{16}\mathcal{F},$$
$$C_{12}=C_{21}=\frac{3}{8}{r_0}^2\left(\frac{\partial^2\phi_{ij}}{\partial r^2}\right)_0-\frac{1}{16}\mathcal{F},$$
$$C_{33}=2(C_{11}-C_{12})=\frac{3}{2}{r_0}^2\left(\frac{\partial^2\phi_{ij}}{\partial r^2}\right)_0+\frac{1}{4}\mathcal{F},$$

(a3)

and

$$D_{11}=D_{22}=\frac{3}{4}{r_0}^2\left[3\left(\frac{\partial\phi_{ij}}{\partial\cos\theta}\right)_0-14\left(\frac{\partial\phi_{ij}}{\partial\cos\varphi}\right)_0\right],$$
$$D_{12}=D_{21}=\frac{3}{4}{r_0}^2\left[3\left(\frac{\partial\phi_{ij}}{\partial\cos\theta}\right)_0+2\left(\frac{\partial\phi_{ij}}{\partial\cos\varphi}\right)_0\right],$$
$$D_{33}=2(D_{11}-D_{12})=-24\left(\frac{\partial\phi_{ij}}{\partial\cos\varphi}\right)_0,$$

(a4)

and

$$\mathcal{F}=9(1-F)^2\left[4\left(\frac{\partial\phi_i^S}{\partial\cos\theta}\right)_0+6\left(\frac{\partial^2\phi_i^S}{\partial\cos\theta^2}\right)_0-3\left(\frac{\partial^2\phi_i^S}{\partial\cos\theta\partial\cos\theta'}\right)_0\right]-36r_0(1-F^2)\left(\frac{\partial^2\phi_i^S}{\partial r\partial\cos\theta}\right)_0+6F(F+2){r_0}^2\left(\frac{\partial^2\phi_{ij}}{\partial r^2}\right)_0.$$

(a5)

Then the conditions of positive definiteness of **C** and **D** become

$$\begin{matrix}C_{11}+C_{12}>0\\C_{11}-C_{12}>0\end{matrix}\rightarrow\begin{matrix}\left(\frac{\partial^2\phi_{ij}}{\partial r^2}\right)_0>0,\\6{r_0}^2\left(\frac{\partial^2\phi_{ij}}{\partial r^2}\right)_0+\mathcal{F}>0,\end{matrix}$$

(a6)

and

$$\begin{matrix}D_{11}+D_{12}>0\\D_{11}-D_{12}>0\end{matrix}\rightarrow\begin{matrix}\left(\frac{\partial\phi_i^S}{\partial\cos\theta}\right)_0-2\left(\frac{\partial\phi_i^S}{\partial\cos\varphi}\right)_0>0,\\\left(\frac{\partial\phi_i^S}{\partial\cos\varphi}\right)_0<0.\end{matrix}$$

(a7)

For BH materials, the in-plane shift vector **η** and out-of-plane shift ζ are determined by

$$\frac{\partial\Phi}{\partial\eta_\gamma}=\sum_{\alpha,\beta}\left(\frac{\partial^2\Phi}{\partial\varepsilon_{\alpha\beta}\partial\eta_\gamma}\varepsilon_{\alpha\beta}+\frac{\partial^2\Phi}{\partial\kappa_{\alpha\beta}\partial\eta_\gamma}\kappa_{\alpha\beta}\right)+\sum_\alpha\frac{\partial^2\Phi}{\partial\eta_\alpha\partial\eta_\gamma}\eta_\alpha+\frac{\partial^2\Phi}{\partial\zeta\partial\eta_\gamma}\zeta=0,$$
$$\frac{\partial\Phi}{\partial\zeta}=\sum_{\alpha,\beta}\left(\frac{\partial^2\Phi}{\partial\varepsilon_{\alpha\beta}\partial\zeta}\varepsilon_{\alpha\beta}+\frac{\partial^2\Phi}{\partial\kappa_{\alpha\beta}\partial\zeta}\kappa_{\alpha\beta}\right)+\sum_\alpha\frac{\partial^2\Phi}{\partial\eta_\alpha\partial\zeta}\eta_\alpha+\frac{\partial^2\Phi}{\partial\zeta^2}\zeta=0.$$

(a8)

Eq. (a8) yields eq. (35) where G and H are

$$G=\frac{9a_0^2\left(2h_0^2+a_0^2\right)\left(\frac{\partial^2V_3}{\partial\cos\theta^2}\right)_0-2r_0^6\left(\frac{\partial^2V_2}{\partial r^2}\right)_0}{r_0^6\left(\frac{\partial^2V_2}{\partial r^2}\right)_0+9a_0^4\left(\frac{\partial^2V_3}{\partial\cos\theta^2}\right)_0},$$

(a9)

and

$$H=\frac{-a_0^2r_0^6\left(\frac{\partial^2V_2}{\partial r^2}\right)_0+18h_0^2a_0^4\left(\frac{\partial^2V_3}{\partial\cos\theta^2}\right)_0}{2h_0^2\left[r_0^6\left(\frac{\partial^2V_2}{\partial r^2}\right)_0+18a_0^4\left(\frac{\partial^2V_3}{\partial\cos\theta^2}\right)_0\right]},$$

(a10)

where

$$\frac{\partial^2V_3}{\partial\cos\theta^2}=\frac{1}{2}\left(\frac{\partial^2V_3}{\partial\cos\theta_A{}^2}+\frac{\partial^2V_3}{\partial\cos\theta_B{}^2}\right).$$

(a11)

In substituting eqs. (20) and (35) into eq. (34), we have the elements of **C** and **D**:

$$C_{11}=C_{22}=C_1^B+\mathcal{H}+\mathcal{G},$$
$$C_{12}=C_{21}=C_2^B+\mathcal{H}-\mathcal{G},$$

(a12)

and

$$D_{11}=D_{22}=\frac{81h_0^2a_0^4}{8r_0^4}\left(\frac{\partial^2V_3}{\partial\cos\theta^2}\right)_0,$$
$$D_{12}=D_{21}=\frac{27h_0^2a_0^4}{8r_0^4}\left(\frac{\partial^2V_3}{\partial\cos\theta^2}\right)_0,$$

(a13)

where

$$C_1^B=\frac{9a_0^4}{8r_0^2}\left(\frac{\partial^2V_2}{\partial r^2}\right)_0+\frac{27a_0^4\left(12h_0^4+4h_0^2a_0^2+a_0^4\right)}{16r_0^8}\left(\frac{\partial^2V_3}{\partial\cos\theta^2}\right)_0,$$

(a14)

$$C_2^B=\frac{3a_0^4}{8r_0^2}\left(\frac{\partial^2V_2}{\partial r^2}\right)_0+\frac{27a_0^4\left(4h_0^4-4h_0^2a_0^2-a_0^4\right)}{16r_0^8}\left(\frac{\partial^2V_3}{\partial\cos\theta^2}\right)_0,$$

(a15)

$$\mathcal{H}=\frac{3H\left(Hh_0^2+a_0^2\right)h_0^2}{r_0^2}\left(\frac{\partial^2V_2}{\partial r^2}\right)_0+\frac{54H(H-1)h_0^4a_0^4}{r_0^8}\left(\frac{\partial^2V_3}{\partial\cos\theta^2}\right)_0,$$

(a16)

and

$$\mathcal{G}=\frac{3(G+2)Ga_0^4}{8r_0^2}\left(\frac{\partial^2V_2}{\partial r^2}\right)_0+\frac{27G\left[4h_0^2+(2-G)a_0^2\right]a_0^6}{8r_0^8}\left(\frac{\partial^2V_3}{\partial\cos\theta^2}\right)_0.$$

(a17)

Then the conditions of positive definiteness of **C** and **D** become

$$\begin{matrix} C_{11}+C_{12}>0 \\ C_{11}-C_{12}>0 \end{matrix} \rightarrow \begin{matrix} C_1^{\mathrm{B}}+C_2^{\mathrm{B}}+2\mathcal{H}>0, \\ C_1^{\mathrm{B}}-C_2^{\mathrm{B}}+2\mathcal{G}>0, \end{matrix} \tag{a18}$$

and

$$\begin{matrix} D_{11}+D_{12}>0 \\ D_{11}-D_{12}>0 \end{matrix} \rightarrow \left(\frac{\partial^2 V_3}{\partial\cos\theta^2}\right)_0>0. \tag{a19}$$

For 2H-MX_2 materials, the in-plane shift vector $\boldsymbol{\eta}^{\pm}$ and out-of-plane shift $\zeta^{\pm}$ are determined by

$$\begin{aligned} \frac{\partial\Phi}{\partial\eta_\gamma^\sigma} &= \sum_{\alpha,\beta}\left(\frac{\partial^2\Phi}{\partial\varepsilon_{\alpha\beta}\partial\eta_\gamma^\sigma}\varepsilon_{\alpha\beta}+\frac{\partial^2\Phi}{\partial\kappa_{\alpha\beta}\partial\eta_\gamma^\sigma}\kappa_{\alpha\beta}\right) \\ &\quad+\sum_{\alpha,\sigma'}\frac{\partial^2\Phi}{\partial\eta_\alpha^{\sigma'}\partial\eta_\gamma^\sigma}\eta_\alpha^{\sigma'}+\sum_{\sigma'}\frac{\partial^2\Phi}{\partial\zeta^{\sigma'}\partial\eta_\gamma^\sigma}\zeta^{\sigma'}=0, \\ \frac{\partial\Phi}{\partial\zeta^\sigma} &= \sum_{\alpha,\beta}\left(\frac{\partial^2\Phi}{\partial\varepsilon_{\alpha\beta}\partial\zeta^\sigma}\varepsilon_{\alpha\beta}+\frac{\partial^2\Phi}{\partial\kappa_{\alpha\beta}\partial\zeta^\sigma}\kappa_{\alpha\beta}\right) \\ &\quad+\sum_{\alpha,\sigma'}\frac{\partial^2\Phi}{\partial\eta_\alpha^{\sigma'}\partial\zeta^\sigma}\eta_\alpha^{\sigma'}+\sum_{\sigma'}\frac{\partial^2\Phi}{\partial\zeta^{\sigma'}\partial\zeta^\sigma}\zeta^{\sigma'}=0. \end{aligned} \tag{a20}$$

Eq. (a18) yields eq. (39) where I, J, L and M are

$$\begin{aligned} &I=\frac{i}{A+B},\ J=\frac{j}{A-B}, \\ &L=\frac{l}{P+2B},\ W=\frac{w}{P-2B}, \end{aligned} \tag{a21}$$

where

$$\begin{aligned} \frac{\partial^2 V_3}{\partial\cos\theta_1{}^2} &= \frac{\partial^2 V_3}{\partial\cos\theta_{\mathrm{M_1X_n^\sigma X_m^\sigma}}{}^2}, \\ \frac{\partial^2 V_3}{\partial\cos\theta_2{}^2} &= \frac{\partial^2 V_3}{\partial\cos\theta_{\mathrm{M_1X_n^\sigma X_n^{\sigma'}}}{}^2}, \\ \frac{\partial^2 V_3}{\partial\cos\theta_3{}^2} &= \frac{\partial^2 V_3}{\partial\cos\theta_{\mathrm{X_l^\sigma M_n M_m}}{}^2}, \end{aligned} \tag{a22}$$

$$\begin{aligned} i &= \frac{27a_0{}^6\left(2d_0{}^2+a_0{}^2\right)}{8r_0{}^8}\left(\frac{\partial^2 V_3}{\partial\cos\theta_1{}^2}+\frac{\partial^2 V_3}{\partial\cos\theta_3{}^2}\right)_0 \\ &\quad-\frac{12d_0{}^4a_0{}^4}{r_0{}^8}\left(\frac{\partial^2 V_3}{\partial\cos\theta_2{}^2}\right)_0-\frac{3a_0{}^4}{2r_0^2}\left(\frac{\partial^2 V_2}{\partial r^2}\right)_0, \end{aligned} \tag{a23}$$

$$\begin{aligned} j &= \frac{3d_0a_0{}^4}{4r_0^2}\left(\frac{\partial^2 V_2}{\partial r^2}\right)_0+\frac{27d_0a_0{}^6\left(2d_0{}^2+a_0{}^2\right)}{16r_0{}^8} \\ &\quad\times\left[\left(4d_0{}^2+3a_0{}^2\right)\frac{\partial^2 V_3}{\partial\cos\theta_1{}^2}-a_0{}^2\frac{\partial^2 V_3}{\partial\cos\theta_3{}^2}\right]_0, \end{aligned} \tag{a24}$$

$$\begin{aligned} l &= -\frac{3d_0{}^2a_0{}^4}{2r_0^2}\left(\frac{\partial^2 V_2}{\partial r^2}\right)_0 \\ &\quad+\frac{27d_0{}^4a_0{}^4}{2r_0{}^8}\left(\frac{\partial^2 V_3}{\partial\cos\theta_1{}^2}+\frac{\partial^2 V_3}{\partial\cos\theta_3{}^2}\right)_0 \\ &\quad+\frac{27d_0{}^4a_0{}^4}{2r_0{}^8}\left(\frac{\partial^2 V_3}{\partial\cos\theta_2{}^2}\right)_0, \end{aligned} \tag{a25}$$

$$\begin{aligned} w &= \frac{3d_0{}^3a_0^2}{4r_0^2}\left(\frac{\partial^2 V_2}{\partial r^2}\right)_0 \\ &\quad-\frac{27d_0{}^3a_0{}^4}{4r_0{}^8}\left[\left(2d_0{}^2+a_0{}^2\right)\frac{\partial^2 V_3}{\partial\cos\theta_1{}^2}-a_0{}^2\frac{\partial^2 V_3}{\partial\cos\theta_3{}^2}\right]_0, \end{aligned} \tag{a26}$$

$$\begin{aligned} A &= \frac{3a_0{}^4}{2r_0^2}\left(\frac{\partial^2 V_2}{\partial r^2}\right)_0+\frac{27a_0{}^8}{8r_0{}^8}\left(\frac{\partial^2 V_3}{\partial\cos\theta_1{}^2}+\frac{\partial^2 V_3}{\partial\cos\theta_3{}^2}\right)_0 \\ &\quad+\frac{6d_0{}^4a_0{}^4}{r_0{}^8}\left(\frac{\partial^2 V_3}{\partial\cos\theta_2{}^2}\right)_0, \end{aligned} \tag{a27}$$

$$B=\frac{6d_0{}^4a_0{}^4}{r_0{}^8}\left(\frac{\partial^2 V_3}{\partial\cos\theta_3{}^2}\right)_0, \tag{a28}$$

and

$$\begin{aligned} P &= \frac{3d_0{}^4}{r_0^2}\left(\frac{\partial^2 V_2}{\partial r^2}\right)_0+\frac{27d_0{}^4a_0{}^4}{r_0{}^8}\left[\frac{\partial^2 V_3}{\partial\cos\theta_1{}^2}+\frac{\partial^2 V_3}{\partial\cos\theta_3{}^2}\right]_0 \\ &\quad+\frac{12d_0{}^4a_0{}^4}{r_0{}^8}\left(\frac{\partial^2 V_3}{\partial\cos\theta_2{}^2}\right)_0. \end{aligned} \tag{a29}$$

In substituting eqs. (23) and (39) into eq. (38), we have the elements of **C** and **D**:

$$\begin{aligned} C_{11} &= C_{22}=C_1^{\mathrm{H}}+\mathcal{L}+\mathcal{I}, \\ C_{12} &= C_{21}=C_2^{\mathrm{H}}+\mathcal{L}-\mathcal{I}, \end{aligned} \tag{a30}$$

and

$$\begin{aligned} D_{11} &= D_{22}=D_1{}^{\mathrm{H}}+\mathcal{W}+\mathcal{J}, \\ D_{12} &= D_{21}=D_1{}^{\mathrm{H}}+\mathcal{W}-\mathcal{J}, \end{aligned} \tag{a31}$$

where

$$\begin{aligned} C_1^{\mathrm{H}} &= \frac{9a_0{}^4}{4r_0^2}\left(\frac{\partial^2 V_2}{\partial r^2}\right)_0+\frac{18d_0{}^4a_0{}^4}{r_0{}^8}\left(\frac{\partial^2 V_3}{\partial\cos\theta_2{}^2}\right)_0 \\ &\quad+\frac{27a_0{}^4\left(12d_0{}^4+4d_0{}^2a_0{}^2+a_0{}^4\right)}{16r_0{}^8} \\ &\quad\times\left(\frac{\partial^2 V_3}{\partial\cos\theta_1{}^2}+\frac{\partial^2 V_3}{\partial\cos\theta_3{}^2}\right)_0, \end{aligned} \tag{a32}$$

$$\begin{aligned} C_2^{\mathrm{H}} &= \frac{3a_0{}^4}{4r_0^2}\left(\frac{\partial^2 V_2}{\partial r^2}\right)_0+\frac{6d_0{}^4a_0{}^4}{r_0{}^8}\left(\frac{\partial^2 V_3}{\partial\cos\theta_2{}^2}\right)_0 \\ &\quad-\frac{27a_0{}^4\left(-4d_0{}^4+4d_0{}^2a_0{}^2+a_0{}^4\right)}{16r_0{}^8} \\ &\quad\times\left(\frac{\partial^2 V_3}{\partial\cos\theta_1{}^2}+\frac{\partial^2 V_3}{\partial\cos\theta_3{}^2}\right)_0, \end{aligned} \tag{a33}$$

$$\begin{aligned} \mathcal{L} &= \frac{3Ld_0{}^2\left(a_0{}^2+Ld_0{}^2\right)}{r_0^2}\left(\frac{\partial^2 V_2}{\partial r^2}\right)_0 \\ &\quad+\frac{48(L-1)Ld_0{}^4a_0{}^4}{r_0{}^8}\left(\frac{\partial^2 V_3}{\partial\cos\theta_2{}^2}\right)_0 \\ &\quad+\frac{54(L-1)Ld_0{}^4a_0{}^4}{r_0{}^8}\left(\frac{\partial^2 V_3}{\partial\cos\theta_1{}^2}+\frac{\partial^2 V_3}{\partial\cos\theta_3{}^2}\right)_0, \end{aligned} \tag{a34}$$

$$\mathcal{I}=\frac{3(I-1)Ia_0^4}{r_0^2}\left(\frac{\partial^2V_2}{\partial r^2}\right)_0+\frac{24(I-1)Id_0^4a_0^4}{r_0^8}\left(\frac{\partial^2V_3}{\partial\cos\theta_2^2}\right)_0+\frac{27I\left[2d^2+a_0^2(1+I)\right]a_0^6}{4r_0^8}\left(\frac{\partial^2V_3}{\partial\cos\theta_1^2}+\frac{\partial^2V_3}{\partial\cos\theta_3^2}\right)_0, \tag{a35}$$

$$D_1^{\mathrm{H}}=\frac{9d^2a_0^4}{16r_0^2}\left(\frac{\partial^2V_2}{\partial r^2}\right)_0+\frac{27d^2a_0^4\left(48d_0^4+56d_0^2a_0^2+17a_0^4\right)}{64r_0^8}\left(\frac{\partial^2V_3}{\partial\cos\theta_1^2}\right)_0+\frac{243d_0^2a_0^8}{64r_0^8}\left(\frac{\partial^2V_3}{\partial\cos\theta_3^2}\right)_0, \tag{a36}$$

$$D_2^{\mathrm{H}}=\frac{3d^2a_0^4}{16r_0^2}\left(\frac{\partial^2V_2}{\partial r^2}\right)_0+\frac{27d^2a_0^4\left(16d_0^4+8d_0^2a_0^2-a_0^4\right)}{64r_0^8}\left(\frac{\partial^2V_3}{\partial\cos\theta_1^2}\right)_0+\frac{189d_0^2a_0^8}{64r_0^8}\left(\frac{\partial^2V_3}{\partial\cos\theta_3^2}\right)_0, \tag{a37}$$

$$\mathcal{W}=\frac{3Wd_0^3\left(2Wd_0-a_0^2\right)}{r_0^2}\left(\frac{\partial^2V_2}{\partial r^2}\right)_0+\frac{27W\left(2d_0^2+2Wd_0+a_0^2\right)d_0^3a_0^4}{r_0^8}\left(\frac{\partial^2V_3}{\partial\cos\theta_1^2}\right)_0+\frac{27W\left(2Wd_0-a_0^2\right)d_0^3a_0^4}{r_0^8}\left(\frac{\partial^2V_3}{\partial\cos\theta_3^2}\right)_0, \tag{a38}$$

and

$$\mathcal{J}=\frac{3J(d_0+2J)a_0^4}{r_0^2}\left(\frac{\partial^2V_2}{\partial r^2}\right)_0+\frac{27J\left(4d_0^3+3d_0a_0^2-2Ja_0^2\right)a_0^6}{8r_0^8}\left(\frac{\partial^2V_3}{\partial\cos\theta_1^2}\right)_0+\frac{27J(d_0+2J)a_0^8}{8r_0^8}\left(\frac{\partial^2V_3}{\partial\cos\theta_3^2}\right)_0. \tag{a39}$$

Then the conditions of positive definiteness of **C** and **D** become

$$\begin{matrix}C_{11}+C_{12}>0\\C_{11}-C_{12}>0\end{matrix}\rightarrow\begin{matrix}C_1^{\mathrm{H}}+C_2^{\mathrm{H}}+2\mathcal{L}>0,\\C_1^{\mathrm{H}}-C_2^{\mathrm{H}}+2\mathcal{I}>0,\end{matrix} \tag{a40}$$

and

$$\begin{matrix}D_{11}+D_{12}>0\\D_{11}-D_{12}>0\end{matrix}\rightarrow\begin{matrix}D_1^{\mathrm{H}}+D_2^{\mathrm{H}}+2\mathcal{W}>0,\\D_1^{\mathrm{H}}-D_2^{\mathrm{H}}+2\mathcal{J}>0.\end{matrix} \tag{a41}$$